Defocused imaging of UV-driven surface-bound molecular motors

Defocused imaging of UV-driven surface-bound molecular motors

Bartosz Krajnik[1†], Jiawen Chen[2†], Matthew A. Watson[3†], Scott L. Cockroft[3], Ben L. Feringa[2*] and Johan C. Hofkens[1*]

1. Molecular Imaging and Photonics, Department of Chemistry, Katholieke Universiteit Leuven, Leuven, Belgium

2. Centre for Systems Chemistry, Stratingh Institute for Chemistry, University of Groningen, The Netherlands

3. EaStCHEM School of Chemistry, University of Edinburgh, Joseph Black Building, David Brewster Road, Edinburgh, EH9 3FJ, U.K..

Supporting Information Placeholder

ABSTRACT: Synthetic molecular motors continue to attract great interest due to their ability to transduce energy into nanomechanical motion, the potential to do work and drive systems out-of-equilibrium. Of particular interest are unidirectional rotary molecular motors driven by chemical fuel or light. Probing the mechanistic details of their operation at the single-molecule level is hampered by the diffraction limit, which prevents the collection of dynamic positional information by traditional optical methods. Here we use defocused wide-field imaging to examine the unidirectional rotation of individual molecular rotary motors on a quartz surface in unprecedented detail. The sequential occupation of nanomechanical states during the UV and heat-induced cycle of rotation are directly imaged in real-time. The approach will undoubtedly prove important in elucidating the mechanistic details and assessing the utility of novel synthetic molecular motors in the future.

Many techniques offer insight into the operation of molecular machines at an ensemble level.[1-5] Advanced techniques can reveal sub-diffraction limit detail.[6-8] Translational and rotational motion of relatively large biological motors can even be monitored at the single-molecule level.[9-11] However, such approaches often require complicated methods for synchronizing molecular behavior, and the dynamics of individual molecules, including the ordering of events and reverse steps often cannot be observed. Indeed, as the dimensions of chemical bonds are well below the diffraction limit of light, direct imaging of mechanistic detail at the single-bond level still presents a great challenge not easily met with optical methods.[12, 13] Defocused wide-field imaging allows the diffraction limit to be circumvented.[14] The orientation of individual fluorophores can be determined from the pattern of photons projected beyond the focal plane of the object upon laser excitation.[15, 16] Defocused imaging has been used to study rotational diffusion in polymers,[17] the relative orientations of emitters in dendrimers,[18, 19] ligand-protein interactions,[20] membrane organization [21] and the optical biasing of surface-bound molecular rotors.[22] Furthermore, the approach enables simultaneous observation of multiple emitters and multi-colour imaging. We sought to take inspiration from the seminal study in which the rotary motion of single ATPase protein motors was directly observed in real-time.[11] We addressed the challenge of monitoring the rotation of an individual synthetic light-driven molecular rotary motor and elucidating the details of the rotary cycle.

We present defocused wide-field imaging studies that show the UV-driven rotation of surface-bound molecular motors (Figure 1). Molecular motors based on overcrowded alkenes have been extensively investigated at an ensemble level and are capable of performing macroscopic work via their collective unidirectional rotation when aligned at interfaces and within other anisotropic environments like liquid crystals or polymer gels.[23-26] The mechanism of rotation has been well studied both theoretically[27] and experimentally.[28] As such, they provide an ideal model system to demonstrate the capacity of defocused wide-field imaging to examine dynamic nanomechanical behavior at the single-molecule level. The structure of motor **1** is shown in Figure 1a.[29] The upper half of the motor, which serves as the rotor, is appended with a bright, stable perylene diimide fluorophore.

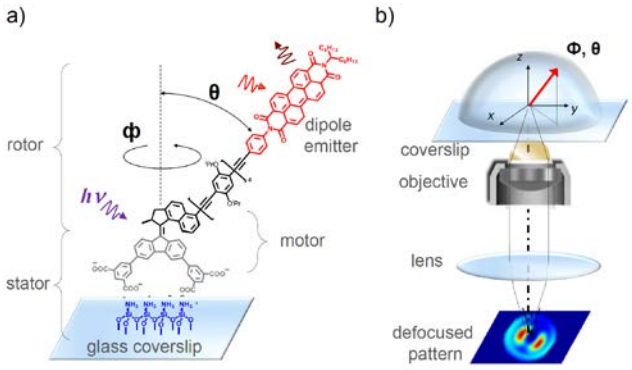

Figure 1. a) Structure of the surface-bound molecular motor (motor **1**) used in the present study. When irradiated with UV light the rotor underwent rotation in the plane of the glass via a series of kinetically trapped states that have different orientations relative to the initial position of the rotor. **b**) The orientations were revealed via wide-field defocused fluorescence microscopy.[23, 27] followed by matching of the experimentally determined emission patterns to calculated model patterns.

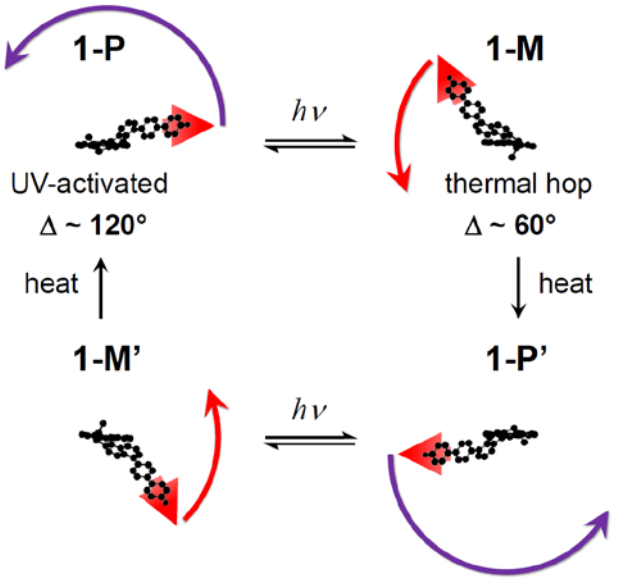

Figure 2. Unidirectional rotation of molecular motor **1** (single enantiomer shown). In solution, the motor rotates through a four-state cycle involving photochemical isomerization steps (purple arrows) each followed by an irreversible thermal helix inversion step (red arrows), involving relative changes of in-plane-angle of ~120° and ~60°, respectively. The large red arrows indicate the orientation of the dipole emitter.

A rigid phenyl-ethylene oligomer linker was used to prevent possible fluorescence quenching between the motor core and the dipole emitter. The lower half of the motor bears tetrapodal carboxylate legs permitting the motor to be grafted to an amine-coated glass surface via electrostatic interactions, and was considered as the stator. The modified glass surface was coated with a spin-cast polymer film to protect the emitters from environmental degradation and to slow rotation to a rate that permitted resolution of the different states. One laser (λ_{ex} = 375 nm) drove rotation of the motor molecules, while a second laser (λ_{ex} = 532 nm) induced fluorescence of the dipoles.

The fluorescence from a single emitter is structured and anisotropic in space. A displacement of the microscope objective by ~ 1 μm with respect to the focal plane of the emitters allowed the angular distribution of the emitted fluorescence to be translated into an intensity pattern on the detector, which revealed information about the 3D orientation of the transition dipole moment of the emitter (Figure 1b). The expected emission pattern for every angular distribution of photons in terms of the in-plane (ϕ) and out-of-plane (θ) angular component can be calculated simply. Thus, fitting and cross-correlation of the measured to calculated patterns enabled the orientations of the individual emitters to be derived.

The UV-driven unidirectional rotation of the motor core is shown in Figure 2. In a racemic population of motors, both enantiomers are present and thus, across the population unidirectional rotation in both senses occurs. Here, anti-clockwise rotation of the rotor is depicted relative to the stator which is considered fixed for simplicity (Figure 2). The molecule is depicted as for surface bound motors seen through an inverted microscope; looking through the stator along the axis of rotation. Upon UV irradiation, a photochemical isomerization of the central double bond occurs, which results in a ~120° in-plane rotation of the rotor from the initial state **1-P**. The obtained state **1-M** is unstable due to high steric strain. The molecule can exit this unstable state by

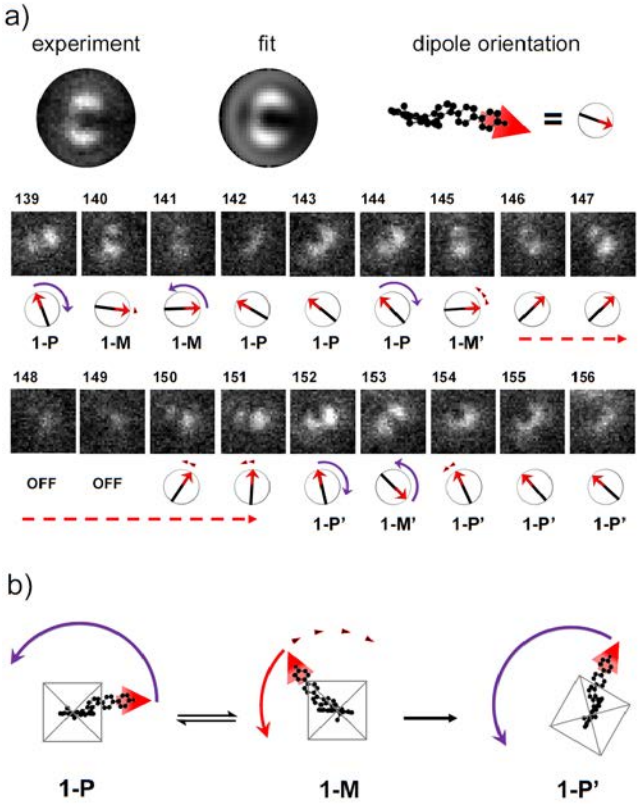

Figure 3. **a**) Experimental defocused patterns of surface-bound motors were fitted to a library of calculated patterns to derive the in-plane and out-of-plane angles describing the orientation of the dipoles and thus the relative nanomechancial state in each frame. The data were recorded with an integration time of 200 ms at 27±3°. The dipoles exhibited successive photo-isomerizations of the rotor (purple arrows Δϕ ~ 120°) and smaller changes Δϕ ~ 1 – 60° (red arrowheads). **b)** Suggested interpretation of the optomechanical response for surface-bound motors. The net unidirectional rotation of the rotor relative to the stator was masked due to work done by the motors causing the entire molecule (motor and tetrapodal base indicated by the grey crossed square) to rotate relative to the surface during the helicity inversion steps (red arrows) in the opposite sense to the rotor.

photo-isomerization back to **1-P** (the *E-Z* photo-isomerization is fully reversible under constant laser irradiation) or via a thermally-activated helix inversion (THI) step, which involves a ~60° in-plane rotation of the rotor, affording a more stable state **1-P'.** Photo-isomerization to **1-M'** followed by THI to **1-P** completes the rotary cycle. Concurrent laser excitation of the motors and the fluorophores was performed and data recorded with an integration time of 200 ms. The general relationship between the defocused pattern and the in-plane orientation is indicated at the top of Figure 3a; the dipole bisects the crescent pattern and points towards the gap between the two bright lobes. An extract of sequential emission patterns recorded for a single dynamic and long-lived emitter and the corresponding orientations derived from the in-plane angle (ϕ) is presented frame-by-frame. A video of the raw data are provided in the supporting information (supporting video 1). Defocused imaging of individual emitters showed that when motor **1** was bound to a surface via exchangeable electrostatic interactions, net unidirectional rotation of motor **1** was obscured. Under UV excitation, the dipoles were observed to undergo re-orientations with both in-

plane (ϕ) and out-of-plane (θ) angular components. Large changes Δϕ ~ 120° in both directions were observed, consistent with reversible photo-isomerization between **P** and **M** or **P'** and **M'** states. Smaller fluctuations ± 1-10° were also observed, presumably due to thermal noise. Crucially, the sequence of events in Figure 3.a exemplified by frames 144 - 163 shows two successive photo-isomerizations (fast Δϕ ~120°) that occured in the same sense (clockwise) separated by slow change due to thermal motion. This sequence of events revealed the occurrence of a complete optomechanical cycle of rotation of the rotor relative to the stator. However, the change in ϕ during the thermal (slow) transition between these photo-isomerizations was counter-clockwise. Inspection of the recordings of several motors (supporting videos 1- 6) showed the behavior was common. We propose that the whole molecule may be rotating relative to the surface as in Figure 3b due to transient dissociation and reassociation of the feet with the surface during the ratcheted THI step.

The distribution of orientations exhibited by this dipole are shown in Figure 4a. The concentration of points at ϕ ~ 130°, θ ~ 45° corresponds to frames recorded prior to inititiating UV irradiation. Under UV irradiation, both ϕ and θ angles were observed to change and the full range of ϕ angles were exhibited indicating complete rotations of the motor. The white lines connecting successive points show frequent jumps of Δϕ ~ 120° corresponding to photo-isomerizations. Meanwhile, θ was usually between 20 – 50° with respect to vertical (θ = 0°). The changes in θ were consistent with the reorientation of the dipole during passage of the naphthalene moiety of the rotor across the stator. The distribution of ϕ angles for this motor suggests three symmetrically arranged orientations, consistent with combination of net clockwise reorientations due to photo-isomerization and retrograde motion of the entire molecule during the THI steps. Across the population of motors, the relative occupation of the **M**, **M'**, **P** and **P'** states in terms of ϕ angle was occluded by the random orientations of the motors on the surface combined with the retrograde in-plane motion and the different number of measurements made for individual motors. However, the θ angles associated with each state are unchanged by the relative in-plane orientations of the motor molecules. Hence, direct measurement of θ angles from a population of surface-bound molecular motors (N>15000, n = 77) revealed the relative occupation of **M+M'** and **P+P'** states (Figure 4b). The data show substantial population of the **M+M'** states (θ = 31.0 ± 5.4°), consistent with the system being driven away from equilibrium by laser irradiation.[30] This population of states contrasts with that at equilibrium where **M+M'** states would be expected to be negligible (figure S6).

In conclusion, we have demonstrated the utility of wide-field defocused imaging to gain insight into the dynamic behavior of synthetic molecular rotary motors at interfaces. Application of the technique to a well-studied class of motor enabled us to showcase the capacity of defocused wide-field imaging to deliver mechanistic insight at the single-molecule level and even the dynamics of an individual carbon-carbon bond that would be opaque to ensemble-level methods. We have shown that the unidirectional rotary behavior of the motor was modulated upon electrostatic attachment to a surface. Our measurements suggest that work was performed by the motors as they returned to equilibrium during the ratcheted thermal helicity inversion step to rotate the entire molecule relative to the surface. We expect that the present work will help to inform the design of more advanced surface-anchored systems based on UV-driven molecular motors. Particularly if unidirectional rotation is to be harnessed, the molecule must be fixed to the surface in such a way that it cannot counter-rotate; perhaps by multiple covalent linkages. Furthermore, we anticipate that wide- field defocused imaging will come to further prominence in investigations of the efficiency, limitations and thus the potential utility of synthetic molecular motors at interfaces.

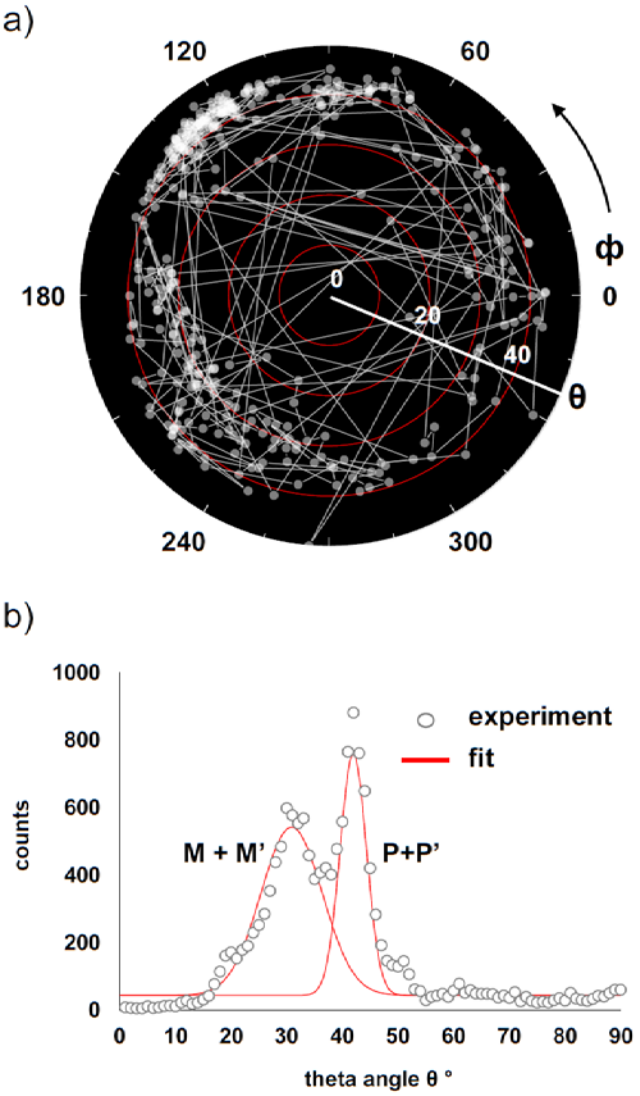

Figure 4. a) Distribution of all the orientations exhibited by a typical motor. The circumferential axis denotes the in-plane angular component (ϕ) while the radial axis denotes the out-of-plane angular component (θ) of each derived dipole orientation. White lines indicate the change in orientation between successive frames. **b**) Occupation of the θ angles derived across a population of measured dipole orientations (N > 15000, n = 77). The data were fitted to normal distributions (R^2 = 0.93) with centers at 31.0 ± 5.4° (**M+M'**) and 42.0 ± 2.3° (**P+P'**) consistent with the expected attachment of the motors to the surface.

ASSOCIATED CONTENT

Supporting Information

Characterization of motor **1**, experimental data. This material is available free of charge via the Internet at http://pubs.acs.org.

AUTHOR INFORMATION

Corresponding Author

Johan C. Hofkens (johan.hofkens@kuleuven.be)
Ben L. Feringa (b.l.feringa@rug.nl);

Author Contributions

†these authors contributed equally.

Notes

The authors declare no competing financial interests.

ACKNOWLEDGMENT

B.K. thanks the Polish Ministry of Science and Higher Education's Mobility Plus programme (1068/MOB/2013/0). M.W. and S.L.C. thank the Engineering and Physical Sciences Research Council (EP/H021620-1) and the ERC (Starting Grant 336935, "Trans-membrane molecular machines") for financial support. B.L.F. thanks the ERC (Advanced Grant No. 694345) and the Netherlands Ministry of Education, Culture and Science (Gravity program 024.001.035) for financial support.

REFERENCES

(1) (a) Stoddart, J. F., *Acc. Chem. Res.*, **2000**, *100*, 409-522. (b) Jimenez, M. C.; Dietrich-Buchecker, C.; Sauvage, J. P., *Angew. Chem. Int. Ed.*, **2000**, *39*, 3284-3287. (c) Balzani, V.; Venturi, M.; Credi, A., *Molecular Devices and Machines - A Journey into the Nanoworld*; Wiley-VCH: Weinheim, **2003**. (d) Kinbara, K.; Aida, T., *Chem. Rev.*, **2005**, *105*, 1377-1400. (e) Kottas, G. S.; Clarke, L. I.; Horinek D.; Michl, J., *Chem. Rev*., **2005**, *105*, 1281-1376. (f) Browne W. R.; Feringa, B. L., *Nat. Nanotechnol.*, 2006, **1**, 25-35. (g) Erbas-Cakmak, S.; Leigh, D. A.; McTernan, C. T.; Nussbaumer, A. L., *Chem. Rev*., **2015**, *115*, 10081-10206.
(2) Koumura, N.; Zijlstra, R. W. J.; van Delden, R. A.; Harada, N.; Feringa, B. L., *Nature*, **1999**, *401*, 152-155.
(3) Leigh, D. A.; Wong, J. K. Y.; Dehez, F.; Zerbetto, F., *Nature*, **2003**, *424*, 174-179.
(4) Berna, J.; Leigh, D. A.; Lubomska, M.; Mendoza, S. M.; Perez, E. M.; Rudolf, P.; Teobaldi, G.; Zerbetto, F., *Nat. Mater.*, **2005**, *4*, 704-710.
(5) Watson, M. A.; Cockroft, S. L., *Chem. Soc. Rev.*, **2016**. *45*, 6118-6129.
(6) Uttamapinant, C.; Howe, J. D.; Lang, K.; Beránek, V.; Davis, L.; Mahesh, M.; Barry, N. P.; Chin, J. W., *J. Am. Chem. Soc.*, **2015**, *137*, 4602-4605.
(7) Saurabh, S.; Perez, A. M.; Comerci, C. J.; Shapiro, L.; Moerner, W. E., *J. Am. Chem. Soc.*, **2016**, *138*, 10398-10401.
(8) Huang, B.; Jones, S. A.; Brandenburg, B.; Zhuang, X., *Nat. Meth.*, **2008**, *5*, 1047-1052.
(9) Yildiz, A.; Forkey, J. N.; McKinney, S. A.; Ha, T.; Goldman, Y. E.; Selvin, P. R., *Science*, **2003**, *300*, 2061-2065.
(10) Reck-Peterson, S. L.; Derr, N. D.; Stuurman, N., *Cold Spring Harb. Protoc.*, **2010**, *2010*, (3), pdb.top73.
(11) Adachi, K.; Yasuda, R.; Noji, H.; Itoh, H.; Harada, Y.; Yoshida, M.; Kinosita, K., *Proc. Natl. Acad. Sci. USA*, **2000**, *97*, 7243-7247.
(12) de Oteyza, D. G.; Gorman, P.; Chen, Y.-C.; Wickenburg, S.; Riss, A.; Mowbray, D. J.; Etkin, G.; Pedramrazi, Z.; Tsai, H.-Z.; Rubio, A.; Crommie, M. F.; Fischer, F. R., *Science*, **2013**, 340, 1434-1437.
(13) Stipe, B. C.; Rezaei, M. A.; Ho, W., *Science*, **1998**, *279*, 1907-1909.
(14) Uji-i, H.; Deres, A.; Muls, B.; Melnikov, S.; Enderlein, J.; Hofkens, J., *Fluorescence of Supermolecules, Polymers, and Nanosystems*, Berberan-Santos, M. N., Ed. Springer Berlin Heidelberg: Berlin, Heidelberg, **2008**; pp 257-284.
(15) Böhmer, M.; Enderlein, J., *J. Opt. Soc. Am. B*, **2003**, *20*, 554-559.
(16) Lieb, M. A.; Zavislan, J. M.; Novotny, L., *J. Opt. Soc. Am. B*, **2004**, *21*, 1210-1215.
(17) Uji-i, H.; Melnikov, S. M.; Deres, A.; Bergamini, G.; De Schryver, F.; Herrmann, A.; Müllen, K.; Enderlein, J.; Hofkens, J., *Polymer*, **2006**, *47*, 2511-2518.
(18) Schroeyers, W.; Vallée, R.; Patra, D.; Hofkens, J.; Habuchi, S.; Vosch, T.; Cotlet, M.; Müllen, K.; Enderlein, J.; De Schryver, F. C., *J. Am. Chem. Soc.*, **2004**, *126*, 14310-14311.
(19) Melnikov, S. M.; Yeow, E. K. L.; Uji-i, H.; Cotlet, M.; Müllen, K.; De Schryver, F. C.; Enderlein, J.; Hofkens, J., *J. Phy. Chem. B*, **2007**, *111*, 708-719.
(20) Osborne, M. A., *J. Phy. Chem. B*, **2005**, *109*, 18153-18161.
(21) Armendariz, K. P.; Huckabay, H. A.; Livanec, P. W.; Dunn, R. C., *Analyst*, **2012**, *137*, 1402-1408.
(22) Hutchison, J. A.; Uji-i, H.; Deres, A.; Vosch, T.; Rocha, S.; Muller, S.; Bastian, A. A.; Enderlein, J.; Nourouzi, H.; Li, C.; Herrmann, A.; Mullen, K.; De Schryver, F.; Hofkens, J., *Nat. Nanotechnol.*, **2014**, *9*, 131-136.
(23) Kudernac, T.; Ruangsupapichat, N.; Parschau, M.; Macia, B.; Katsonis, N.; Harutyunyan, S. R.; Ernst, K.-H.; Feringa, B. L., *Nature*, **2011**, *479*, 208-211.
(24) Eelkema, R.; Pollard, M. M.; Vicario, J.; Katsonis, N.; Ramon, B. S.; Bastiaansen, C. W. M.; Broer, D. J.; Feringa, B. L., *Nature*, **2006**, *440*, 163-163.
(25) Li, Q.; Fuks, G.; Moulin, E.; Maaloum, M.; Rawiso, M.; Kulic, I.; Foy, J. T.; Giuseppone, N., *Nat. Nanotechnol.*, **2015**, *10*, 161-165.
(26) Klok, M.; Boyle, N.; Pryce, M. T.; Meetsma, A.; Browne, W. R.; Feringa, B. L., *J. Am. Chem. Soc.*, **2008**, *130*, 10484-10485.
(27) Kazaryan, A.; Kistemaker, J. C. M.; Schäfer, L. V.; Browne, W. R.; Feringa, B. L.; Filatov, M., *J. Phy. Chem. A*, **2010**, *114*, 5058-5067.
(28) Conyard, J.; Cnossen, A.; Browne, W. R.; Feringa, B. L.; Meech, S. R., *J. Am. Chem. Soc.*, **2014**, *136*, 9692-9700.
(29) For the analytical data of **1**, see supporting information. Detailed design, synthesis and isomerization studies will be reported separately.
(30) Outliers at much larger θ angles may indicate transient detachment from the surface during energetic transitions or motors that were poorly attached due to local variations in the polymer layer.

Insert Table of Contents artwork here